Charge separation at liquid interfaces

Arghya Majee [1], Christoph A. Weber [2,*] and Frank Jülicher [1,3,4,†]

[1] *Max Planck Institute for the Physics of Complex Systems, 01187 Dresden, Germany*

[2] *Faculty of Mathematics, Natural Sciences, and Materials Engineering: Institute of Physics, University of Augsburg, Universitätsstrasse 1, 86159 Augsburg, Germany*

[3] *Center for Systems Biology Dresden, 01307 Dresden, Germany*

[4] *Cluster of Excellence Physics of Life, TU Dresden, 01062 Dresden, Germany*

(Received 4 December 2023; accepted 11 July 2024; published 5 August 2024)

We present a theory for phase-separated liquid coacervates with salt, taking into account spatial heterogeneities and interfacial profiles. We find that charged layers of alternating sign can form around the interface while the bulk phases remain approximately charge neutral. We show that the salt concentration regulates the number of layers and the amplitude of the layer's charge density and electrostatic potential. Such charged layers can either repel or attract single-charged molecules diffusing across the interface. Our theory could be relevant for artificial systems and biomolecular condensates in cells. Our work suggests that interfaces of biomolecular condensates could mediate charge-specific transport similar to membrane-bound compartments.

DOI: 10.1103/PhysRevResearch.6.033138

I. INTRODUCTION

Spatial organization of macromolecules is essential for regulating cellular processes. Most biochemical processes involve charged macromolecules like DNA, RNA, and proteins that are immersed in a multicomponent, aqueous electrolyte solution containing various salt ions. These biomolecules assemble into specific compartments that provide unique environments to perform certain tasks [1,2]. Moreover, compartmentalization of prebiotic components and chemical reactions was also proposed as a selection mechanism at the origin of life [3–6].

Compartments in cells can either be membrane-bound, or membrane-less liquid droplets that can disperse and reform for varying conditions in cells [7–9]. Such intracellular droplets are called biomolecular condensates and often form via liquid-liquid phase separation [1,2,10,11]. Many biomolecular condensates in cells contain negatively charged RNA and positively charged proteins [12], suggesting coacervation as a mechanism underlying their formation [13]. Indeed, *in vitro* experiments show that condensate properties are strongly affected by salt concentration [14–16]. Coacervates are liquid droplets composed of charged macromolecules and counterions interacting via electrostatic interactions. In physical chemistry, they are classified into two categories [17]: *simple* coacervates formed by a single type of macroion and its counterions, and *complex* coacervates due to electrostatic interactions between oppositely charged macroions. Coacervation as a mechanism to spatially organize and select molecules was already proposed at the beginning of the 20th century as an organizing principle for the molecular origin of life [3,4].

A first theoretical model for coacervates was proposed by Overbeek and Voorn [18]. Within this model, phase separation results from a competition between the mixing entropy and the electrostatic interactions between the oppositely charged molecules, which is described using the Debye-Hückel approximation in the Poisson-Boltzmann equation treating ions as dilute components. However, when coacervates form, charged macromolecules and salt ions are in general nondilute and interactions among all charged components are essential, in particular at physiological conditions. Interactions were shown to indeed affect the distribution of macroions close to charged surfaces [19,20]. Most theories on electrolytes study flat and colloidal charged surfaces that are solid [21,22]. In contrast, coacervates provide phase boundaries separating liquid phases that are soft and permeable.

Recent experimental studies show that coacervate phase boundaries give rise to rich physical behavior [14,23–27]. Condensates can carry a surface charge and thus move in an applied electric field due to electrophoresis [24,26–28]. The surface charge and the associated ζ potential were also recognized as one of the factors determining droplet stability [26]. Not only that, the interfacial tension of protein droplets depends on salinity as well as on the Donnan potential difference that exists between two coexisting phases [14,29]. Such studies indeed highlight the importance of electrostatics and interfaces in phase-separated, coacervate systems. Recently, Zhang and Wang have proposed a theory that can explain the origin of interfacial charges in asymmetric complex coacervates [30]. This work closely parallels the concepts provided by Onuki [31] for partitioning of diluted salt with asymmetries in Born solvation energies across phases in binary mixtures.

*Contact author: christoph.weber@physik.uni-augsburg.de

†Contact author: julicher@pks.mpg.de

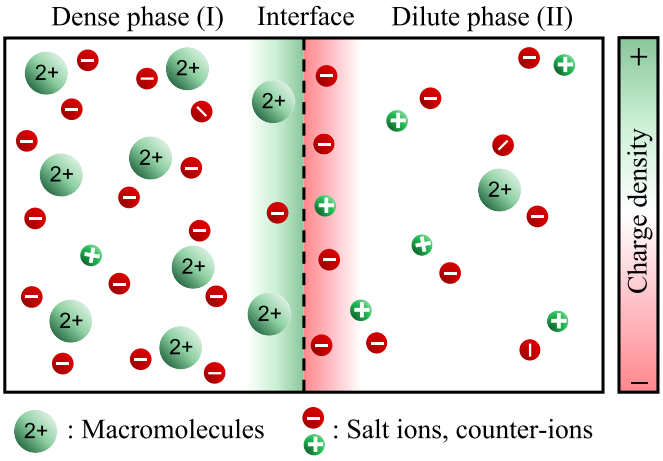

FIG. 1. Schematics of the considered phase-separated electrolyte mixtures. Macromolecule-rich phases (phase I) can form in an initially homogeneous saline solution with macromolecules (big green circles). Macromolecules are depicted to be positively charged, with counterions being anions. Dissociation of salts also generate co/counterions. Charges can separate with a charge density that deviates from electroneutrality, particularly around the interface (indicated by the color gradients).

In this work we present a theoretical framework similar to Refs. [30–32] and apply it to nondilute mixtures composed of charged macromolecules and salt ions capable of forming coexisting phases, i.e., a coacervate phase-separated from a dilute phase. We account for the mean-field electrostatic interactions among all charged components and study the concentration profiles of components in each phase and in the interfacial domain. Our key finding is that charge separation occurs at the interface, while each phase is approximately charge neutral (see an illustration in Fig. 1), both for symmetric and asymmetric complex coacervates as well as for simple coacervates. The corresponding electrostatic potential shows a nonmonotonic behavior with attractive wells and repulsive barriers. Strikingly, the electrostatic potential can also give rise to multiple layers of alternating charges. This implies that charged molecules may exhibit a complex transition kinetics through coacervate interfaces. We also present an analytical calculation to investigate the charge oscillations in the bulk phases and identify competing length scales of different physical origins that lead to such oscillatory profiles.

II. ELECTROTHERMODYNAMICS OF PHASE SEPARATION

We consider an electrolyte mixture composed of charged macromolecules and counterions that can phase separate into a macromolecule-rich and a macromolecule-poor phase; see Fig. 1 for an illustration. Each component, $i = 1, ..., M$, can carry a molecular charge $q_i e$, with e denoting the positive elementary charge. Here we consider constant charge for each component and for simplicity do not account for chemical processes leading to charge regulation [33–35]. Moreover, the electrolyte mixture is considered to be incompressible, corresponding to constant molecular volumes v_i. Incompressibility implies that the condition $\sum_{i=1}^{M} v_i n_i(\mathbf{x}) = 1$ holds locally, where $n_i(\mathbf{x})$ denotes the concentration field of component i at position $\mathbf{x}$. At constant temperature and pressure, this condition reduces the thermodynamic description to $(M-1)$ independent concentration fields $n_i(\mathbf{x})$.

All the components in the mixture collectively generate a dielectric medium with permittivity $\varepsilon = \varepsilon_r \varepsilon_0$, where ε_0 is the vacuum permittivity and ε_r denotes the relative permittivity, which in general depends on composition $\{n_i\}$. The distributions of charges give rise to an electrostatic potential $\psi(\mathbf{x})$, which is related to the concentrations $n_i(\mathbf{x})$ via the Poisson equation:

$$\nabla \cdot (\varepsilon \nabla \psi) = -\rho, \tag{1a}$$

where $\rho(\mathbf{x}) = \sum_i q_i e n_i(\mathbf{x})$ is the local charge density. The presence of the charges in the system also naturally give rise to a length scale called the Bjerrum length $\ell_B = e^2/(4\pi\varepsilon k_B T)$ specifying the separation at which the Coulombic interaction between two elementary charges becomes comparable to the thermal energy $k_B T$ [20].

The electrothermodynamics of the mixture is governed by the free-energy functional

$$F[n_i, \psi] = \int d^3x \Bigg[f(n_i) + \sum_i \frac{\kappa_i}{2} (\nabla n_i)^2 + \frac{\varepsilon}{2} (\nabla \psi)^2 + \lambda (\nabla \cdot (\varepsilon \nabla \psi) + \rho) + \sum_i \mu_i^{\mathrm{el}} \left(\frac{N_i}{V} - n_i \right) \Bigg], \tag{1b}$$

where f is the free-energy density. Moreover, κ_i is related to the interfacial tension characterizing the energy contribution due to the spatial gradients of the components in the system [36–38]. We refer to κ_i as the gradient cost for component i in the following. We have neglected cross terms of the form $\nabla n_i \cdot \nabla n_j$ for simplicity. The term proportional to $(\nabla\psi)^2$ describes the electrostatic energy density arising from the charged components in the system. Moreover, λ is the Lagrange multiplier to impose that the Poisson Eq. (1a) is satisfied and μ_i^{el} is the Lagrange multiplier fixing the total number of particles $N_i = \int_V d^3x\, n_i(\mathbf{x})$ for each component i with V denoting the volume of the system.

To describe interactions among all components we choose the Flory-Huggins (FH) free-energy density,

$$\frac{f(n_i)}{k_B T} = \sum_{i=1}^{M} (n_i \ln(v_i n_i) + \omega_i n_i) + \sum_{j=2}^{M} \sum_{i=1}^{j-1} \chi_{ij} n_i n_j, \tag{1c}$$

containing the mixing entropy, the internal free energies ω_i, and the mean-field interactions among the charged components of interaction strength χ_{ij} [37,39].

Thermodynamic equilibrium states are characterized by $\delta F/\delta n_i = 0$ and $\delta F/\delta\psi = 0$, leading to

$$\mu_i^{\mathrm{el}} = \frac{\partial f}{\partial n_i} - \kappa_i \nabla^2 n_i + q_i e \psi - \frac{1}{2} \frac{\partial \varepsilon}{\partial n_i} (\nabla\psi)^2, \tag{1d}$$

$$\lambda = \psi. \tag{1e}$$

Here, the constant μ_i^{el} is the exchange electrochemical potential, and the Lagrange multiplier for the Poisson equation is the electrostatic potential ψ. When phases coexist, the value

of $\mu_i^{\rm el}$ corresponds to the slope of the Maxwell construction and the osmotic pressures balance between the phases.

To solve the governing equations [i.e., the Poisson equation and the equations provided by constant exchange electrochemical potential conditions in Eq. (1d)], we use Neumann boundary conditions for the electrostatic potential and the concentrations:

$$(\nabla\psi\cdot\mathbf{n})|_{\partial\Omega}=0, \tag{1f}$$

$$(\nabla n_i\cdot\mathbf{n})|_{\partial\Omega}=0, \tag{1g}$$

where $\mathbf{n}$ is the unit outward normal to the system boundary $\partial\Omega$ enclosing the system volume V. The Neumann boundary condition for the electrostatic potential ensures that the electric field normal to the boundaries vanishes corresponding to zero surface charge. Integrating Poisson Eq. (1a) over the system volume V using the boundary condition (1f) leads to overall electroneutral systems with $\int d^3x\,\rho(\mathbf{x})=0$. Note that we do not impose electroneutrality locally, i.e., $\rho(\mathbf{x})\neq 0$ in general. The Neumann boundary condition for the concentration field corresponds to an inert boundary that has no affinity to adhere or repel components.

In summary, Eq. (1) govern the position-dependent electrothermodynamics of a nondilute mixture composed of charged components where a dense coacervate phase can coexist with a dilute phase. This theoretical framework extends the classical Poisson-Boltzmann theory [22] to nondilute conditions where interactions among the charged components affect the electrostatic potential.

III. RESULTS

In this work we use our theoretical framework given by Eq. (1) to study simple coacervates (Sec. III A) and complex coacervates (Sec. III B). For simplicity, we consider flat interfaces and a one-dimensional system with a position x. We determine the position-dependent electrostatic potential $\psi(x)$ together with concentration fields $n_i(x)$ of all the different charged components. In all studies we use a relative solvent permittivity $\varepsilon_r=80$, corresponding to pure water, and a solvent molecular volume $\nu_s=0.03\,\mathrm{nm}^3$. When salt ions or counterions are present in the system, their molecular volumes are, for simplicity, equal to the solvent. The internal free energies ω_i do not affect the results, as they can be absorbed into the Lagrange multipliers $\mu_i^{\rm el}$. In our studies on simple coacervates, we choose macromolecules carrying a positive charge. In general, macromolecules such as proteins can be positively or negatively charged under physiological conditions. This diversity arises because, for example, the human cytosol has a pH $\simeq 7.2$ [40] and the human proteome shows a bimodal distribution with two major peaks located at pI $\simeq 6.0$ and 8.25 [41].

A. Simple coacervates

1. Minimal model for simple coacervates

We first discuss a minimal model for a simple coacervate that contains a single type of charged macromolecule (p), a neutralizing counterion ($-$), and a solvent component (s). Phase separation in such a system takes place for sufficiently large and positive interaction parameters χ_{ps}. For the numerical examples discussed below, we use $\chi_{ps}=1.5\,\mathrm{nm}^3$ together with $\chi_{-s}=-0.09\,\mathrm{nm}^3$, $\chi_{p-}=-1.0\,\mathrm{nm}^3$, and the volume ratios $\nu_p/\nu_s=\nu_p/\nu_-=20$. The counterions are assumed to be monovalent, e.g., OH^-, with $q_-=-1$, and the macromolecule has a charge $q_p=+3$ if not stated otherwise. For such parameters we numerically solved Eq. (1).

Coexistence of a dense coacervate phase and a dilute phase is reflected in the concentration profiles of charged components $n_i(x)$, which are depicted in Fig. 2(a) for different κ_p/κ_- ratios. Both charged components show a pronounced change highlighting the interface between the dense coacervate phase and the dilute phase. The interface is indicated by a vertical gray dashed line and is defined as the position where the electrostatic potential $\psi(x)$ takes half the value between dense coacervate and dilute phase. The concentration profiles are not symmetric and deviate from the classical interface profile obtained for a symmetric binary Ginzburg-Landau free energy [38,42]. The reason is that the mixture is ternary and molecular volumes of the charged components are different. For decreasing relative gradient cost ratio κ_p (the ratio κ_p/κ_- is varied by only varying κ_p while keeping κ_- fixed), the concentration profiles become steeper around the interface as the energy cost associated with keeping gradients goes down. We also note that although the relative gradient cost ratio κ_p/κ_- is varied by only varying κ_p while keeping κ_- fixed, both n_p and n_- show the same behavior with changing κ_p.

A key finding of our work is that charges can separate within the interfacial domain, which is evident in the spatially varying charge density $\rho(x)$ [Fig. 2(b)]. While the mixture is charge neutral [$\rho(x)\simeq 0$] deep within the dense coacervate and dilute phase, we find multiple domains with a positive or negative charge density. The gradient cost κ_p essentially determines the shape and the amplitudes of the charge density. For the considered parameters there is a pronounced negatively charged domain at $x>0$ and a pronounced positively charged domain at $x<0$.

This separation of charge leads to a complex behavior of the electrostatic potential $\psi(x)$ within the interfacial domain [Fig. 2(c)]. The negatively charged domain at $x>0$ gives rise to a potential well relative to the reference potential in the dilute phase that is chosen to be zero. On the contrary, the positively charged domain at $x<0$ causes a barrier of the electrostatic potential relaxing toward the Donnan potential ψ_D inside the dense phase [43,44]. The electrostatic potential well and barrier implies that a positive test charge would get attracted into the well and repelled by the potential barrier. The existence and strength of both characteristics is set by the cost ration κ_p. For large values, the well and the potential barrier vanish. The reason is that the charge density in the interface approaches concomitantly to zero [Fig. 2(b)] since the free-energy penalty for gradients becomes too large for increasing κ_p.

The charge separation at the interface can be understood in the following way. Due to differences in the interaction between components and their concentration differences in the two phases, a chemical potential difference arises between the phases. To balance this, an electrostatic potential difference between the two phases created by charge separation at the interface develops such that the resulting electrochemical

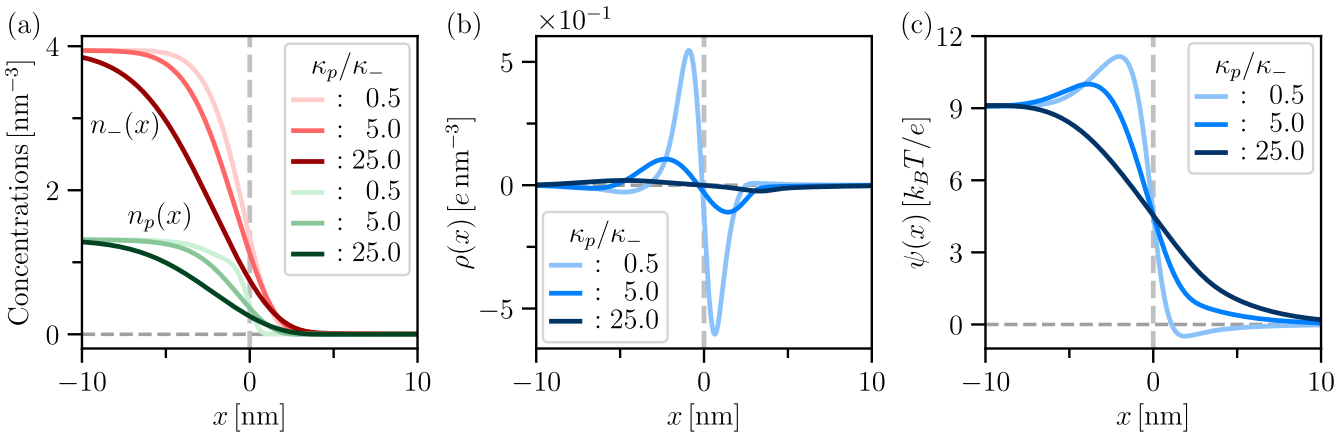

FIG. 2. Interfacial charge separation of simple coacervates without salt. (a) Concentration profiles of charged components $n_i(x)$, where (p) and $(-)$ indicate the macromolecule and counterion, respectively. For increasing κ_p, the profiles steepen around the interface indicated by a vertical dashed line. (b) The charge density $\rho(x) = e[q_p n_p(x) + q_- n_-(x)]$ indicates separation of charged components in the interfacial domain for small enough κ_p. Only in this case, the free-energy penalty is low enough such that interactions of the charged components with the solvent can give rise to a nonzero charge density. (c) The electrostatic potential $\psi(x)$ has a complex shape within the interfacial domain. There is a well in the negatively charged domain and a barrier in the positively charged domain. The potential is set to zero far in the dilute phase. The interface position is defined where the electrostatic potential is half the value deeply inside the dense coacervate phase.

potential becomes equal everywhere. Although not shown here, all the properties presented in Fig. 2 qualitatively remain the same for a system with $\kappa_p/\kappa_- = \nu_p/\nu_- = |q_p/q_-| = \omega_p/\omega_- = 1$, but having slightly different Flory-Huggins interaction parameters. As shown by Aerov *et al.* [32], a similar phenomenon can happen for interfaces separating ionic and nonionic liquids.

2. *Impact of salt on simple coacervates*

Now we consider a system that, in addition to the positively charged macromolecules and its counterions, contains salt. For simplicity, we consider a monovalent salt and do not make any distinction between the counterions and the anions released by the salt. The resulting quaternary mixture thus contains macromolecules (p), cations $(+)$, anions $(-)$, and solvent (s) molecules. For results discussed in this section, we choose the molecular volumes and the interaction parameters as follows: $\nu_p/\nu_s = \nu_p/\nu_+ = \nu_p/\nu_- = 30$, and $\chi_{ps} = 1.9\,\mathrm{nm}^3$, $\chi_{p+} = 1.8\,\mathrm{nm}^3$, $\chi_{p-} = -1.8\,\mathrm{nm}^3$, $\chi_{+-} = \chi_{+s} = \chi_{-s} = -0.09\,\mathrm{nm}^3$. We also set $\kappa_+ = \kappa_- = \kappa$, and unless stated otherwise, use $\kappa = 15\,k_BT\ \mathrm{nm}^5$.

The concentration profiles of charged components $n_i(x)$ in simple coacervates with salt ($i = p, +, -$) show a complex behavior close to the interface [Fig. 3(a)], where the interface is indicated by a vertical dashed line. The macromolecule concentration $n_p(x)$ decreases monotonically, together with the oppositely charged counterion $(-)$ when passing from the dense coacervate phase toward the dilute phase. This coupled behavior is a result of the attractive electrostatic interactions. Interestingly, the positively charged coions $(+)$ vary nonmonotonically, i.e., $(+)$-ions accumulate right outside the coacervate phase. This accumulation is a result of a macromolecule-poor layer right outside the coacervate and is formed by the attractive electrostatic interactions between oppositely charged ions. This variation vanishes with increasing cost ratio κ_p as the profile of macromolecules at the interface flattens and thereby contributes to neutralizing the interfacial domain.

The charge density $\rho(x)$ and the electrostatic potential $\psi(x)$ have a similar qualitative behavior as compared to the case without salt. Multiple charge layers of alternating charge develop within the interfacial region [Fig. 3(b)], and the electrostatic potential can vary nonmonotonically with potential wells and barriers [Fig. 3(c)]. These profile characteristics vanish for increasing κ_p, as it quantifies the free-energy penalty for profile heterogeneities. However, the presence of salt quantitatively makes charge separation more pronounced, i.e., it is observed for even higher values of κ_p.

The well and barrier of the electrostatic potential is determined by the salt concentration c_{salt}. To quantify this impact, we introduce the interfacial potential ψ_{int} as the potential difference between the barrier and the well minimum and contrast it with the Donnan potential ψ_D [Fig. 4(a)]. We also propose a definition for the interface width of the coacervate Δ as the distance between the position of potential well and barrier. We find that the Donnan potential ψ_D and the interfacial potential ψ_{int} decrease with the salt concentration c_{salt} [Fig. 4(b)]. This decrease is due to screening, as more salt reduces the electrostatic interactions of the phase-separated macromolecules. For large salt concentrations, this decrease weakens and crosses over to a logarithmic decay for both ψ_D and ψ_{int}, each decaying with a characteristic salt concentration (see Appendix A). The decrease of ψ_D and ψ_{int} with salt is, however, extremely insensitive to the average macromolecule concentration $\bar{n}_p$. The latter predominantly sets the size of the coacervate without altering the composition significantly. For sufficiently large values of the gradient cost κ_p, the potential profiles become monotonically varying, leading to a vanishing difference $(\psi_{\mathrm{int}} - \psi_D)$ [Fig. 4(c)]; see Fig. 3(c) for the corresponding electrostatic potential profiles. However, lowering the κ_p values leads to barriers and wells of the electrostatic potential and thereby nonzero differences $(\psi_{\mathrm{int}} - \psi_D)$. Interestingly, though both the Donnan potential

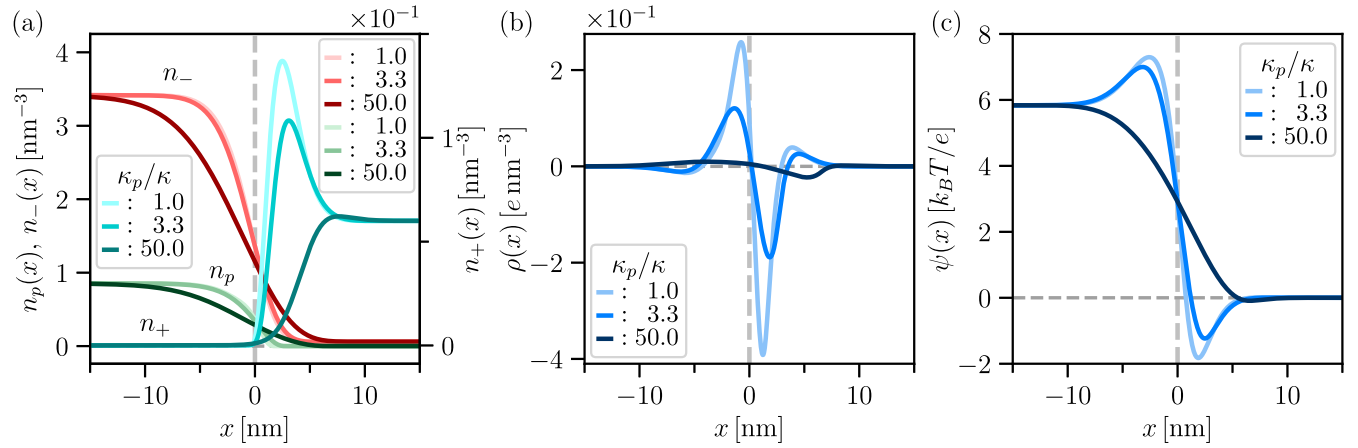

FIG. 3. Interfacial charge separation of simple coacervates with salt. (a) In contrast to the case without salt (Fig. 2), the concentration profiles of charged components $n_i(x)$ ($i = p, -, +$) can vary in a nonmonotonic fashion within the interfacial domain; the interface is indicated by the vertical dashed line. The dense coacervate phase is enriched in positively charged macromolecules together with its neutralizing counterions ($-$), while the positively charged coions ($+$) accumulate adjacent to the interface toward the dilute phase. This accumulation enhances for decreasing κ_p. (b) The charge density $\rho(x) = e[q_p n_p(x) + q_- n_-(x) + q_+ n_+(x)]$ shows, as in the case without salt, that charges separate in the interfacial domain and that charge separation is more pronounced for smaller κ_p. (c) The associated electrostatic potential $\psi(x)$ exhibits potential wells and barriers that are even more pronounced compared to the case without salt. The plots correspond to a system with salt concentration $c_{\text{salt}} = 100\,\text{mM}$, a macromolecular charge $q_p = +4$, and average concentration $\overline{n}_p = 0.1\,\text{mM}$, and ion charges $q_\pm = \pm 1$.

ψ_D and the interfacial potential ψ_{int} decrease with increasing salt, their difference increases [Fig. 4(c)]. This trend indicates that the electrostatic potential differences between the dense coacervate phase and the dilute phase are more affected by salt screening than the interfacial potential. This asymmetry between bulk phases and interfacial domains arises from the additional gradient cost compared to the bulk phases for the counterions to accumulate in the interfacial domains.

The salt concentration determines the amount and the size of the layers within the interfacial domain. A logarithmic representation of the absolute value of the charge density $|\rho(x)|$ reveals that multiple layers of alternating charge extend from the interfacial domain towards the dense and dilute phase, respectively [Fig. 5(a)]. Increasing the salt concentration increases the number of such layers and decreases layer width. To quantify the layering with salt, we calculated the real and imaginary part of $\gamma_{\text{I/II}}$ deeply in the dense coacervate and dilute phase by linearizing the profile of each component i around phase equilibrium n_i^0 by writing

$$n_i(x) = n_i^0 + c_i \exp(\gamma x); \tag{2}$$

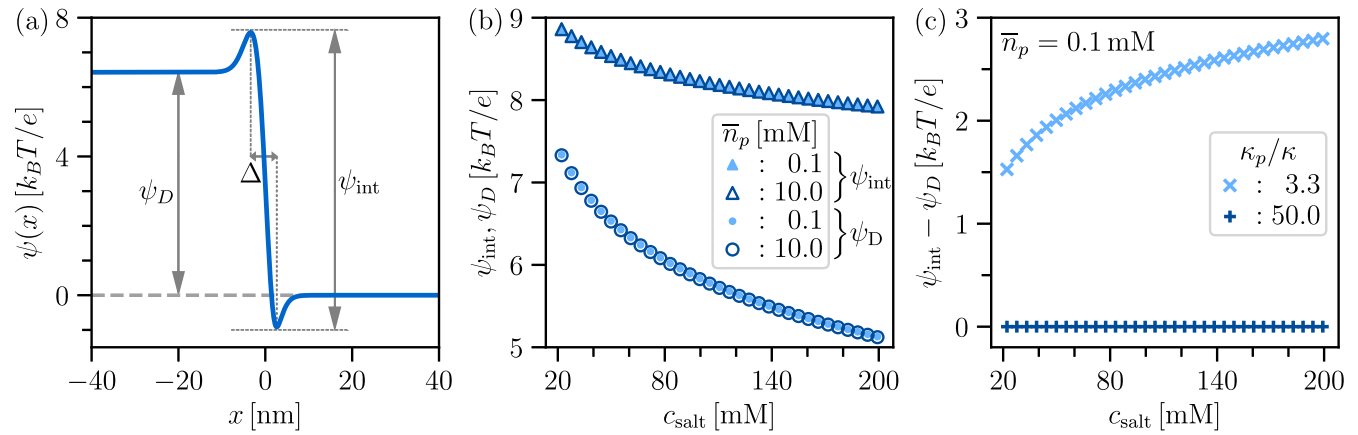

FIG. 4. Impact of salt on the electrostatic potential of simple coacervates. (a) Illustration of the Donnan potential ψ_D, the interfacial potential ψ_{int}, and the interfacial width Δ for a representative electrostatic potential profile $\psi(x)$ obtained for simple coacervates. (b) The Donnan potential ψ_D and the interfacial potential ψ_{int} decrease with salt concentration c_{salt}, since salt screens the electrostatic interactions. The average macromolecule concentration $\overline{n}_p$ in the system hardly affects ψ_D or ψ_{int}, as it mainly alters the size of the dense coacervate phase. (c) For a large value of $\kappa_p = 50$, the potential profile varies monotonically and $\psi_{\text{int}} - \psi_D$ vanishes. Thus, there are no additional potential barriers and wells. For small enough values of κ_p, the difference between Donnan and interfacial potential ψ_{int} and ψ_D is nonzero and increases with salt concentration c_{salt}. The reason is that salt reduces the electrostatic potential by screening, which is more pronounced in the bulk phases due to the ions' gradient costs. We fixed average macromolecule concentration $\overline{n}_p = 0.1\,\text{mM}$. For all the plots here, macromolecule charge $q_p = 4$, and co/counterion charges $q_\pm = \pm 1$ are used.

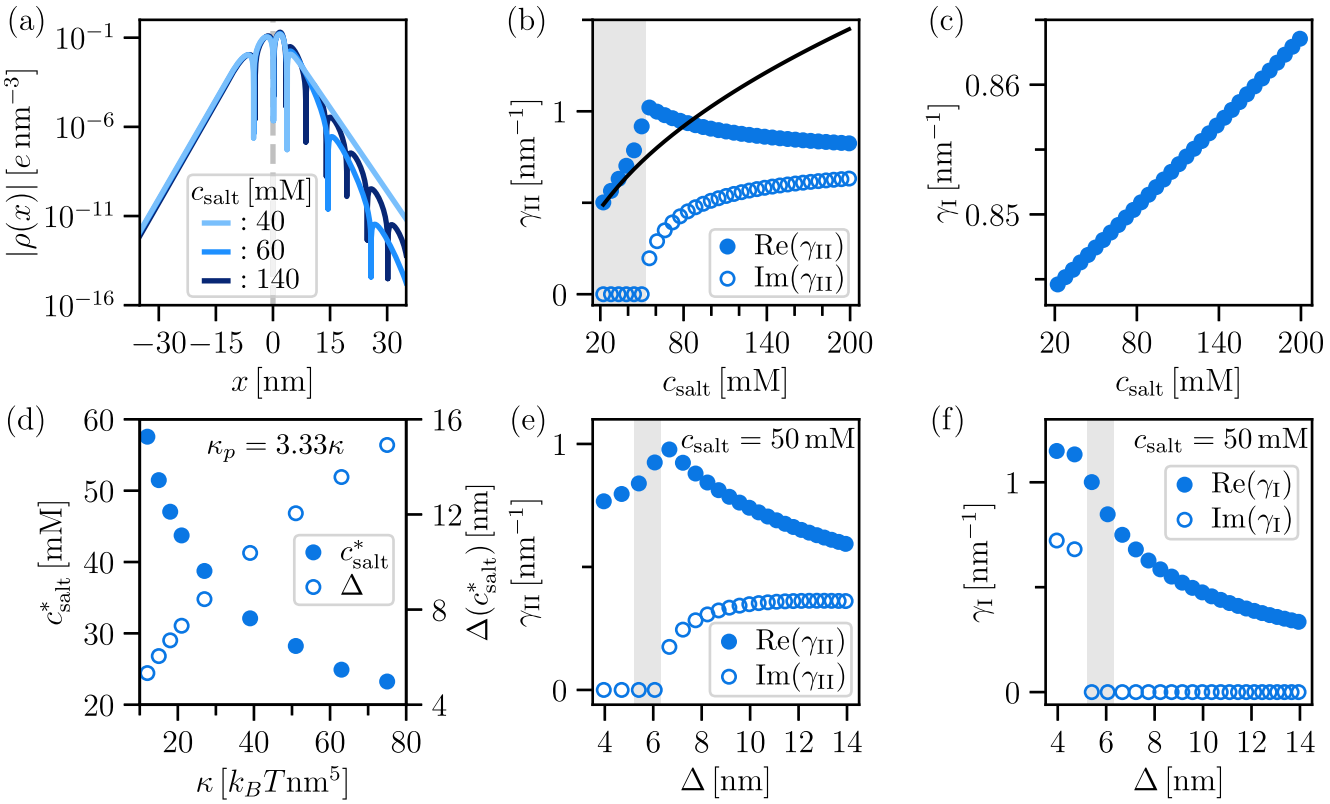

FIG. 5. Layers of alternating charge density in the dense coacervate and dilute phase. (a) Logarithmic representation of the absolute value of the charge density $|\rho(x)|$ around the interfacial domain indicates layers of alternating charge density. The amplitude of charge density $|\rho(x)|$ within layers decays approximately exponentially with characteristic length scales $\mathrm{Re}(\gamma_{\mathrm{I/II}})^{-1}$ that are phase dependent. The width of charged layers that can be characterized by $\mathrm{Im}(\gamma_{\mathrm{I/II}})^{-1}$ decreases with increasing salt concentration c_{salt}. (b) In the dilute phase, $\mathrm{Re}(\gamma_{\mathrm{II}})$ shows a nonmonotonic behavior. A nonzero $\mathrm{Im}(\gamma_{\mathrm{II}})$ indicates the existence of layers of alternating charge. Layers only occur for salt concentrations above the threshold c^*_{salt}. For $c_{\mathrm{salt}} > c^*_{\mathrm{salt}}$, $\mathrm{Re}(\gamma_{\mathrm{I/II}})$ decreases with salt, indicating a deviation from classical Debye-Hückel theory. Here we used $\kappa = 15\,k_BT\,\mathrm{nm}^5$. (c) In the coacervate phase, $\mathrm{Re}(\gamma_{\mathrm{I}})$ changes only weakly with salt, and there are no layers deep in the coacervate phase [$\mathrm{Im}(\gamma_{\mathrm{I}}) = 0$]. (d) The threshold salt concentration c^*_{salt} decreases with increasing interfacial width Δ, where Δ can be changed by the gradient cost κ. (e, f) Increasing the interfacial width Δ makes the system crossing from a situation where alternating charged layers solely exist inside the coacervate, over a regime without any layers, to a regime with layers present exclusively in the dilute phase. For all panels we use $\bar{n}_p = 0.1$ mM, $\kappa_+ = \kappa_- = \kappa$, $\kappa_p = 3.33\kappa$. In panels (e) and (f), the interfacial width Δ is varied by varying κ in the range $(6-75)\,k_BT\,\mathrm{nm}^5$. Further parameters are the same as in Fig. 4. The gray shaded regions in panels (b), (e), and (f) indicate situations where the imaginary part of the decay constant is zero in both phases.

for details see Appendix B. We find that amplitudes of charge density $|\rho(x)|$ in the layers decay approximately exponentially with a characteristics length scale $\mathrm{Re}(\gamma_{\mathrm{I/II}})^{-1}$, an effect reminiscent of classical electrostatic screening as described by the Debye-Hückel theory [45], where $\mathrm{Re}(\gamma)^{-1}$ would correspond to the Debye screening length. For our simple coacervate in the presence of salt, $\mathrm{Re}(\gamma_{\mathrm{II}})$ shows a nonmonotonic behavior with salt [Fig. 5(b)]. For low salt, it increases with increasing salt concentration, which is consistent with Debye-Hückel theory. However, when passing a threshold salt concentration c^*_{salt}, this behavior qualitatively changes as $\mathrm{Re}(\gamma_{\mathrm{II}})$ decreases with increasing salt concentration. The threshold c^*_{salt} coincides with the appearance of a nonzero imaginary part $\mathrm{Im}(\gamma_{\mathrm{II}})$, which indicates the existence of layers of alternating charge also far away from the coacervate interface. In other words, the bulk phases can be layered reminiscent of Coulomb microphase separation in polymer solutions or of block copolymers undergoing microphase separation [46–56], however, noting that the amplitude of charge density decays exponentially when going away from the interface [Fig. 5(a)]. Charged layers, in general, arise due to competing interactions related to different length scales. For our system, these competing length scales are the Bjerrum length ℓ_B, due to electrostatic interactions, and the gradient costs κ_i related to interfacial tension (see Appendix B for details). As derived in Appendix B 5, for a ternary system comprising of oppositely charged species $(+,-)$ in a solvent (s) in the large $\kappa_\pm$ limit, the decay constant γ [defined in Eq. (2)] reads

$$\gamma = \pm\frac{1\pm i}{\sqrt{2}}\left(\frac{e^2}{\varepsilon}\left(\frac{q_+^2}{\kappa_+^2}+\frac{q_-^2}{\kappa_-^2}\right)\right)^{1/4}. \tag{3}$$

Clearly, a competition between the Bjerrum length $\ell_B = e^2/(4\pi\varepsilon k_BT)$ and the length scale associated with the interfacial width gives rise to complex γ, leading to oscillatory number density as well as electrostatic potential profiles.

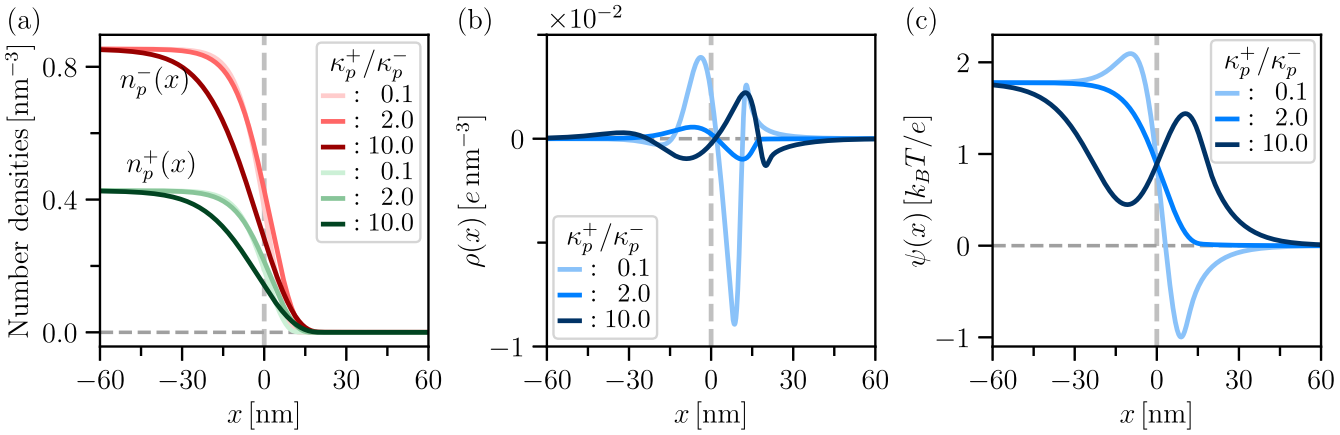

FIG. 6. Interfacial charge separation of complex coacervates. (a) Monotonic decrease of concentration profiles of the macromolecules $n_p^{\pm}(x)$ within the interfacial domain. (b) The charge density $\rho(x) = e[q_p^+ n_p^+(x) + q_p^- n_p^-(x)]$ shows complex spatial variation inside the interfacial domain, indicating that charge separation can also occur for complex coacervation. By altering the relative gradient cost κ_p^+ of the oppositely charged macromolecules, the charged layers can swap their sign. (c) This swapping is evident in the corresponding behavior of the electrostatic potential profile $\psi(x)$ when changing κ_p^+. The ordering of potential barriers and wells swaps. The vertical dashed line in each plot marks the location of the interface. As parameters, we use $q_p^+ = 4$, $q_p^- = -2$ together with other parameters mentioned in Sec. III B.

In the other limit $\kappa_\pm \to 0$, the decay constant is real (see Appendix B for details). While the layering extends to the bulk, the amplitudes of such layers are exponentially damped, implying that the manifestation of layering gets negligible deeply in the respective phases. Moreover, for the considered parameters in Figs. 5(a)–5(c), we have found that layers not necessarily exist in both coexisting phases; here we show an example where the dilute phase is layered while the dense coacervate phase is not [Figs. 5(b) and 5(c)]. Though layers have been reported in theories at charged solid interfaces [57–59], layering around the liquid interface is distinct, as the additional interfacial width is coupled to the spatial variations extending towards both bulk phases.

The interfacial width Δ of the coacervate strongly affects the threshold c^*_{salt} of charge layering [Fig. 5(d)]. The interfacial width can be changed by increasing the parameter characterizing the gradient cost κ, where we chose $\kappa_+ = \kappa_- = \kappa$. Thus, for larger Δ, the threshold for layering, c^*_{salt}, decreases.

The interfacial width Δ also controls whether layers of alternating charge occur in the dilute or in the coacervate phase [Figs. 5(e) and 5(f)]. For low interfacial width Δ the dense coacervate phase [Fig. 5(f)] exhibits layers while the dilute phase does not. Increasing Δ leads to a domain where none of the phases have layers [gray shaded domain in Figs. 5(b), 5(e) and 5(f)]. For even larger value of the interfacial width Δ, the coacervate is not layered while the dilute phase has layers of alternating charge [Fig. 5(e)].

B. Complex coacervates

Here we discuss a minimal model for complex coacervation and scrutinize our key finding of charge separation at the interface. In contrast to a simple coacervate, complex coacervation is driven by the attractive electrostatic interaction between (at least) two oppositely charged macromolecules. As a result, both macromolecule types are enriched inside the coacervate phase compared to the coexisting dilute phase. Our minimal model for a complex coacervate accounts for two oppositely charged macromolecules (p^+ and p^-) suspended in a solvent (s). For the following studies we consider macromolecule-solvent molecular volume ratios $\nu_p^+/\nu_s = \nu_p^-/\nu_s = 20$ and Flory-Huggins parameters $\chi_{p^+s} = 1.0\,\mathrm{nm}^3$, $\chi_{p^-s} = 0.6\,\mathrm{nm}^3$, and $\chi_{p^+p^-} = -1.0\,\mathrm{nm}^3$.

The concentration profiles of the macromolecules $n_p^{\pm}(x)$ vary monotonously [Fig. 6(a)]. We could not find any additional concentration layers as observed for simple coacervates with salt. However, the charge density can exhibit spatial variation in the interfacial domain, indicating that charges can separate also for complex coacervates [Fig. 6(b)]. We have varied the relative gradient cost of the positively to the negatively charged macromolecule, κ_p^+/κ_p^-, by varying κ_p^+. We find that κ_p^+ can flip the charge of the layers when passing through the interfacial domain. For $\kappa_p^+ \ll \kappa_p^-$, the gradients of the concentration field n_p^+ can be steeper compared to those of n_p^-. Therefore, right inside the coacervate one has $n_p^+ > n_p^-$, leading to a positively charged layer. In the other limit, i.e., for $\kappa_p^+ \gg \kappa_p^-$, the gradients of the concentration field n_p^+ become less steep compared to those of n_p^-. Therefore one obtains the swapped case with $n_p^- > n_p^+$ and a negatively charged layer right inside the coacervate. This swapping also becomes evident in the behavior of the electrostatic potential $\psi(x)$ as a function of the relative gradient cost κ_p^+. While for small $\kappa_p^+ \ll \kappa_p^-$, the coacervate phase comprises a potential barrier and the dilute phase a potential well; this swaps for large $\kappa_p^+ \gg \kappa_p^-$.

We end our discussion by commenting on the relevance of changing the gradient costs $\kappa_p^{\pm}$ and some of the parameter choices in our study. Biological condensates are often formed by complex coacervation of two macromolecules of rather different molecular volume, e.g., proteins with oligonucleotides such as RNA and DNA. Moreover, interaction parameters among macromolecules and solvent are generally different.

Since the gradient costs of such macromolecules $\kappa_p^{\pm}$ depend on their molecule volumes and on their interactions, we expect them to vary, suggesting the relevance of our results in Fig. 6 for biomolecular condensates. We also note that our qualitative results, i.e., interfacial charge separation and associated potential profile formation, rely on the asymmetries in Flory-Huggins parameters, and they are expected to be present even for higher macromolecular charges. As to the used model of complex coacervate, in general, free ionic species (e.g., protons) can be present in the solution. However, the resulting quaternary mixture is very much similar to the simple coacervates with the added salt case, albeit with one ionic species being larger. Therefore, we do not expect the qualitative features of our results to change in that case.

IV. CONCLUSIONS

In summary, we present a theoretical framework to study profiles of concentrations and electrostatic potential at interfaces of phase-separated solution containing charged components. We apply this framework to simple and complex coacervates. Our approach extends the Poisson-Boltzmann theory that describes the spatial distributions of ions adjacent to charged, solid surfaces, or charged colloidal particles. In these systems counterions typically follow a Boltzmann distribution and screen the surface charge. Our extension accounts for the interactions among all charged components, taking into account phase coexistence. Our work therefore provides a framework for coacervation at salt concentrations where the Poisson-Boltzmann theory fails [19]. Most importantly, in phase-separated systems, interfaces are associated with free-energy costs for gradients of charged and uncharged components. These contributions are lacking in the classical Poisson-Boltzmann theory.

A similar theoretical framework was recently proposed by Zhang and Wang [30]. However, they focus on electrostatic interaction between charged components and consequently, capture interfacial double-layer formation for the case of asymmetric complex coacervates. We show that the phenomenon of interfacial charge separation is much more general and can take place in any system with asymmetric interaction between components. We also show that charge separation can take place away from the interface due to a competition between the interfacial length scales and the Bjerrum length.

The key finding of our theory is therefore the general presence of charge separation in the interfacial domain of *any* type of coacervates, be it simple or complex. Beyond a threshold salt concentration, multiple layers of alternating charges can occur around the interface, which extends into the bulk phases. However, the amplitude of the charge contained in each layer decreases exponentially for increasing distance from the interface. We show that salt regulates the number and the width of such layers of alternating charges. Similar layering has also previously been reported, but in homogeneous systems for large salt concentrations. Charge layering in such homogeneous systems results from correlations beyond mean-field as well as within mean-field description [57–64]. Our studies show that layering can occur at the mean-field level with moderate salt concentrations due to phase separation where the interfacial width controls the layer patterns.

Charged layers localized around the interface can affect interfacial transport. An interesting case is the stochastic trajectory of single-charged probe molecules diffusing across the interface. This molecule will encounter the electric potential profile with barriers and traps, which affects the transport kinetics. The resulting charge-specific reflection or trapping of the probe at the interface suggests charge-dependent transport properties at the interface. In the context of biomolecular condensates forming via phase separation in cells [1], this phenomenon could be used by cells to regulate molecular transport, a property usually associated with membranes [65,66].

Our finding of complex-shaped charged layers at the coacervate interfaces implies that a coacervate is not a colloid with a surface charge surrounded by a (dilute) layer of screening counterions. Counterions at coacervate interfaces are, in general, nondilute and participate in the phase separation equally as the macromolecules. In other words, the surface charge is not solely a property of the coacervate, as is typically the case for colloids. For coacervates, the surface charge depends on the interactions and concentrations of all charged components in the system. Thus, changes in salt or gradient costs alter the coacervate's surface charge and the screening counterion distribution. This complexity poses an exciting challenge in calculating the electrophoretic mobility when coacervates are subject to external electric fields [24,26,28].

Our theoretical framework also paves the way to investigating even more complex phase separation phenomena in nondilute mixtures composed of charged components. It remains elusive why coacervates hardly undergo coarsening by Ostwald ripening [17,67,68], and why coacervates can repel each other or stick without fusing [69]. Moreover, the surface charge of coacervates could also be regulated by pH [33–35], and coacervates can also act as chemical reactors [70–72]. Recently, coacervates maintained away from equilibrium were shown to deform to complex shapes, including the formation of liquid shells [73,74].

Finally, we note that, for simplicity, we have combined a Flory-Huggins model with long-range electrostatic interactions to discuss profiles of interfacial charges. However, other approaches have been proposed that also account for an electrostatic free energy beyond mean field, as well as chain correlations along polymer [30,75–78]. It will be interesting to include such effects in our analysis and additionally account for charge regulation of macromolecules [33,34] to investigate how the charge oscillations at and away from the coacervate interface are affected.

ACKNOWLEDGMENTS

We thank L. Hubatsch for fruitful discussion on the topics of interfacial transport, P. M. McCall for general discussions on electrostatics of protein droplets, and M. Bier and S. Dietrich for discussions on the oscillatory behavior of charge and density profiles. F.J. acknowledges funding by the Volkswagen Foundation. C.A.W. acknowledges the European Research Council (ERC) for financial support under the European Union's Horizon 2020 Research and Innovation Program ("Fuelled Life" with Grant Agreement No. 949021).

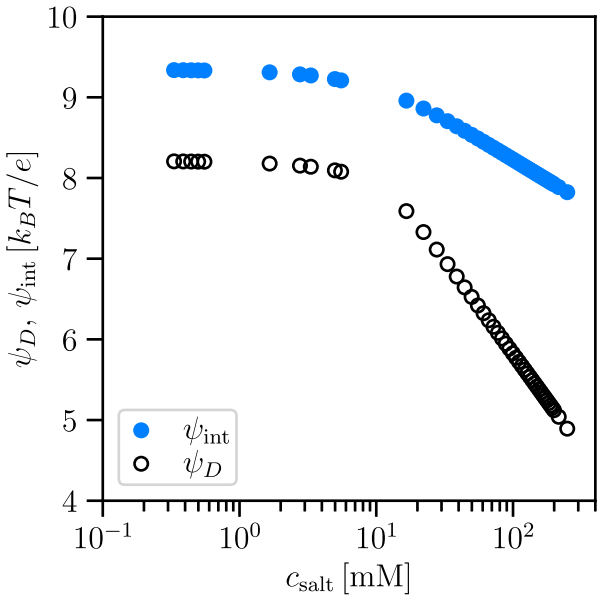

FIG. 7. Variation of both the Donnan potential ψ_D and the interfacial potential $\psi_{\rm int}$ [defined in Fig. 4(a)] as functions of the salt concentration $c_{\rm salt}$, showing that ψ_D and $\psi_{\rm int}$ vary logarithmically for large $c_{\rm salt}$ but with different rates.

APPENDIX A: ψ_D AND $\psi_{\rm int}$ AS A FUNCTION OF SALT CONCENTRATION

In Fig. 4 of the main text, we have shown the variations of the Donnan potential ψ_D and the interfacial potential $\psi_{\rm int}$ as functions of the salt concentration $c_{\rm salt}$ using linear scales. In order to gain further insight into the actual variation, we plot them for an even larger salt concentration range using semi-log scale in Fig. 7. As the plots suggest, both ψ_D and $\psi_{\rm int}$ vary logarithmically with $c_{\rm salt}$ but with different rates.

APPENDIX B: DECAYING CHARGE OSCILLATIONS TOWARDS BULK PHASES

1. Governing equations

Let us consider a ternary system consisting of a positively charged species (+), a negatively charged species (−), and a solvent (s). Conservation of volume fractions implies that all of the three volume fractions are not independent of each other. As always, we consider the one for the solvent to be the dependent one, which is given by $(1-\nu_+n_+-\nu_-n_-)$. The other two volume fractions, or equivalently, the corresponding concentration profiles (as we consider constant molecular volumes $\nu_\pm$), together with the electrostatic potential everywhere in the system, can be obtained by solving the following equations:

$$\nabla^2\psi = -\frac{\rho}{\varepsilon}, \tag{B1}$$

$$\mu_\pm^{\rm el} = \text{constant}. \tag{B2}$$

2. Exponential ansatz and small deviation assumption

Away from the interface, all the quantities decay exponentially as

$$n_+ = n_+^0 + c_+\exp(\gamma x) + \text{c.c.}, \tag{B3}$$

$$n_- = n_-^0 + c_-\exp(\gamma x) + \text{c.c.}, \tag{B4}$$

$$\psi = \psi^0 + c_\psi\exp(\gamma x) + \text{c.c.}, \tag{B5}$$

to their respective bulk values, i.e., to n_+^0, n_-^0, and ψ^0 with a decay constant γ. Here, c.c. refers to the complex conjugate. As there are three equations to solve for four unknowns (c_+, c_-, c_ψ, and γ), one can obtain only the ratios $c_p = c_+/c_\psi$ and $c_m = c_-/c_\psi$. Inserting the exponential profiles [Eqs. (B3)–(B5)] back into the Poisson equation (B1), one obtains the condition

$$\gamma^2 = -\frac{e(q_+c_p + q_-c_m)}{\varepsilon}. \tag{B6}$$

As c_+, c_-, and c_ψ are not restricted to be real valued, both c_p and c_m, and consequently, γ, can also be complex valued. Please note that a complex γ corresponds to oscillatory profiles for the number densities and the electrostatic potential. Next, the exponential profiles are inserted into the equal exchange electrochemical potential conditions [Eq. (B2)]. The log terms are expanded up to linear order with respect to small deviations from the bulk densities [i.e., in $\exp(\gamma x)$] in the following way:

$$\begin{aligned}\log(\nu_i n_i) &= \log\left[\nu_i n_i^0 + \nu_i c_i\exp(\gamma x)\right]\\ &= \log\left[\nu_i n_i^0\left(1+\frac{c_i}{n_i^0}\exp(\gamma x)\right)\right]\\ &= \log\left(\nu_i n_i^0\right) + \log\left(1+\frac{c_i}{n_i^0}\exp(\gamma x)\right)\\ &= \log\left(\nu_i n_i^0\right) + \frac{c_i}{n_i^0}\exp(\gamma x) + \cdots,\end{aligned}$$

and

$$\begin{aligned}&\log(1-\nu_+n_+-\nu_-n_-)\\ &= \log[1-\nu_+n_+^0-\nu_-n_-^0-(\nu_+c_+-\nu_-c_-)\exp(\gamma x)]\\ &= \log\left[\phi_s^0\left(1-\frac{\nu_+c_+}{\phi_s^0}\exp(\gamma x)-\frac{\nu_-c_-}{\phi_s^0}\exp(\gamma x)\right)\right]\\ &= \log\left(\phi_s^0\right) + \log\left(1-\frac{\nu_+c_+}{\phi_s^0}\exp(\gamma x)-\frac{\nu_-c_-}{\phi_s^0}\exp(\gamma x)\right)\\ &= \log\left(\phi_s^0\right) - \frac{\nu_+c_+}{\phi_s^0}\exp(\gamma x)-\frac{\nu_-c_-}{\phi_s^0}\exp(\gamma x)+\cdots,\end{aligned}$$

where $\phi_s^0 = 1-\nu_+n_+^0-\nu_-n_-^0$. Using these expressions in the constant exchange electrochemical potential conditions and equating the coefficients of $\exp(\gamma x)$ to zero, one obtains

$$\begin{aligned}\kappa_+\gamma^2c_p = &\left[\frac{c_p}{n_+^0}+\frac{\nu_+}{\nu_s}\left(\frac{\nu_+c_p}{\phi_s^0}+\frac{\nu_-c_m}{\phi_s^0}\right)\right]k_BT+\chi_{+-}c_m\\ &-\chi_{+s}\left(2\frac{\nu_+}{\nu_s}c_p+\frac{\nu_-}{\nu_s}c_m\right)-\chi_{-s}\frac{\nu_+}{\nu_s}c_m+eq_+,\end{aligned} \tag{B7}$$

and

$$\kappa_-\gamma^2 c_m = \left[\frac{c_m}{n_-^0} + \frac{\nu_-}{\nu_s}\left(\frac{\nu_+ c_p}{\phi_s^0} + \frac{\nu_- c_m}{\phi_s^0}\right)\right]k_BT + \chi_{+-}c_p - \chi_{-s}\left(2\frac{\nu_-}{\nu_s}c_m + \frac{\nu_+}{\nu_s}c_p\right) - \chi_{+s}\frac{\nu_-}{\nu_s}c_p + eq_-. \tag{B8}$$

Equations (B6), (B7), and (B8) form a set of three equations to be solved for three unknowns c_p, c_m, and γ. We first solve Eqs. (B7) and (B8) to obtain c_p and c_m in terms of γ, and this is then used in Eq. (B6) to obtain the following polynomial equation satisfied by the decay constant γ:

$$\varepsilon\kappa_+\kappa_-\gamma^6 - \varepsilon(a\kappa_- + d\kappa_+)\gamma^4 + (\varepsilon ad - \varepsilon b^2 + e^2q_+^2\kappa_- + e^2q_-^2\kappa_+)\gamma^2 + e^2(2bq_+q_- - q_+^2 d - q_-^2 a) = 0, \tag{B9}$$

where

$$a = \left(\frac{1}{n_+^0} + \frac{\nu_+^2}{\nu_s\phi_s^0}\right)k_BT - 2\chi_{+s}\frac{\nu_+}{\nu_s}, \tag{B10}$$

$$b = \frac{\nu_+\nu_-}{\nu_s\phi_s^0}k_BT + \chi_{+-} - \chi_{+s}\frac{\nu_-}{\nu_s} - \chi_{-s}\frac{\nu_+}{\nu_s}, \tag{B11}$$

$$d = \left(\frac{1}{n_-^0} + \frac{\nu_-^2}{\nu_s\phi_s^0}\right)k_BT - 2\chi_{-s}\frac{\nu_-}{\nu_s}. \tag{B12}$$

Equation (B9) is a polynomial equation of sixth order in γ and can have real as well as complex roots in accordance with what one can already infer from Eq. (B6). A similar calculation can be done for a quaternary system which leads to a polynomial equation of higher degree.

3. Complex decay constant γ

In order to get an idea of the nature and origin of the different roots of γ, we rewrite Eq. (B9) in the following way:

$$\left(\frac{\gamma}{\ell_1}\right)^6 - \left(\frac{\gamma}{\ell_2}\right)^4 + \left(\frac{\gamma}{\ell_3}\right)^2 + r = 0, \tag{B13}$$

with

$$\ell_1^6 = \frac{e^2(q_+^2 d + q_-^2 a - 2bq_+q_-)|_{\chi\to 0}}{\varepsilon\kappa_+\kappa_-}, \tag{B14a}$$

$$\ell_2^4 = \frac{e^2(q_+^2 d + q_-^2 a - 2bq_+q_-)|_{\chi\to 0}}{\varepsilon(a\kappa_- + d\kappa_+)}, \tag{B14b}$$

$$\ell_3^2 = \frac{e^2(q_+^2 d + q_-^2 a - 2bq_+q_-)|_{\chi\to 0}}{\varepsilon ad - \varepsilon b^2 + e^2q_+^2\kappa_- + e^2q_-^2\kappa_+}, \tag{B14c}$$

$$r = \frac{2bq_+q_- - q_+^2 d - q_-^2 a}{(q_+^2 d + q_-^2 a - 2bq_+q_-)|_{\chi\to 0}}. \tag{B14d}$$

The $\chi \to 0$ condition implies that the expression is calculated in the limit of vanishing Flory-Huggins interaction between all components. The resulting limiting expression can be shown to always have a nonzero and strictly positive value. By construction, ℓ_1, ℓ_2, and ℓ_3 are three length scales associated with the roots of γ in Eq. (B9).

Figure 8 shows the variations of these length scales and the corresponding variation of the characteristic length scale $\gamma_{\rm II}$ in the dilute phase as function of the gradient cost for a ternary system (either a simple coacervate without salt, panels (a) and (b), or a complex coacervate, panels (c) and (d)). For both systems, either only one of the gradients costs κ_+ or both of them, i.e., $\kappa_+ = \kappa_- = \kappa$ are varied to change the interfacial width. We note that increasing the gradient cost increases the interfacial width. As one can see from the upper panels of all the plots, with increasing interfacial width, the decay constant $\gamma_{\rm II}$ becomes complex from being purely real. Quite interestingly, the corresponding lower panels suggest that the length scale ℓ_3 also changes its slope around the position where $\gamma_{\rm II}$ changes its behavior. The other two length scales $\ell_{1,2}$ do not manifest such a change. Therefore, the origin of the complex decay constant can be attributed to the length scale ℓ_3, which, as Eq. (B14c) suggests, arises due to a competition of the electrostatic length scale and of the interfacial width. We note that in the limit of vanishing Flory-Huggins interactions $\chi_{ij} \to 0$, vanishing molecular volumes $\nu_\pm \to 0$, and vanishing gradient costs $\kappa_\pm \to 0$, the length scale $\ell_3 = \sqrt{(q_+^2 e^2 n_+^0 + q_-^2 e^2 n_-^0)/(\varepsilon k_BT)}$ matches the well-known inverse Debye length.

4. Criterion for obtaining complex decay rate γ

By using a quadratic variable substitution, Eq. (B9) can be rewritten as a cubic equation which has complex roots for negative discriminant, i.e., for

$$\frac{1}{\ell_2^8\ell_3^4} + \frac{4r}{\ell_2^{12}} - \frac{4}{\ell_1^6\ell_3^6} - \frac{18r}{\ell_1^6\ell_2^4\ell_3^2} - \frac{27r^2}{\ell_1^{12}} < 0. \tag{B15}$$

Consequently, γ can also have complex (with nonzero real part) values only when the condition in (B15) is satisfied.

5. The limits of large and small gradient costs

In the limits of large and small gradient costs, the behavior of the decay constant γ can also be analytically understood.

a. Large gradient costs

In the limit of large gradient costs $\kappa_\pm$, we make the following reasonable ansatz:

$$\gamma \sim \kappa^\alpha, \quad \alpha < 0. \tag{B16}$$

Using this in Eq. (B9), one obtains

$$\mathcal{O}(\kappa^{2+6\alpha}) + \mathcal{O}(\kappa^{1+4\alpha}) + \mathcal{O}(\kappa^{2\alpha}) + \mathcal{O}(\kappa^{1+2\alpha}) + \mathcal{O}(\kappa^0) = 0. \tag{B17}$$

In order to get meaningful solutions for γ, only one term in this expression cannot dominate. Therefore, at least two of the terms scale equally in Eq. (B17), and the remaining ones grow slower. Keeping in mind that $2\alpha < (1 + 2\alpha)$ as well as $(1 + 4\alpha) < (1 + 2\alpha)$ for $\alpha < 0$, one can have the following three situations:

Case I: $\kappa^{2+6\alpha} = \kappa^{1+2\alpha}$. In this case $\alpha = -\frac{1}{4}$, and the polynomial equation (B9) simplifies to

$$\varepsilon\kappa_+\kappa_-\gamma^6 + e^2(q_+^2\kappa_- + q_-^2\kappa_+) \simeq 0.$$

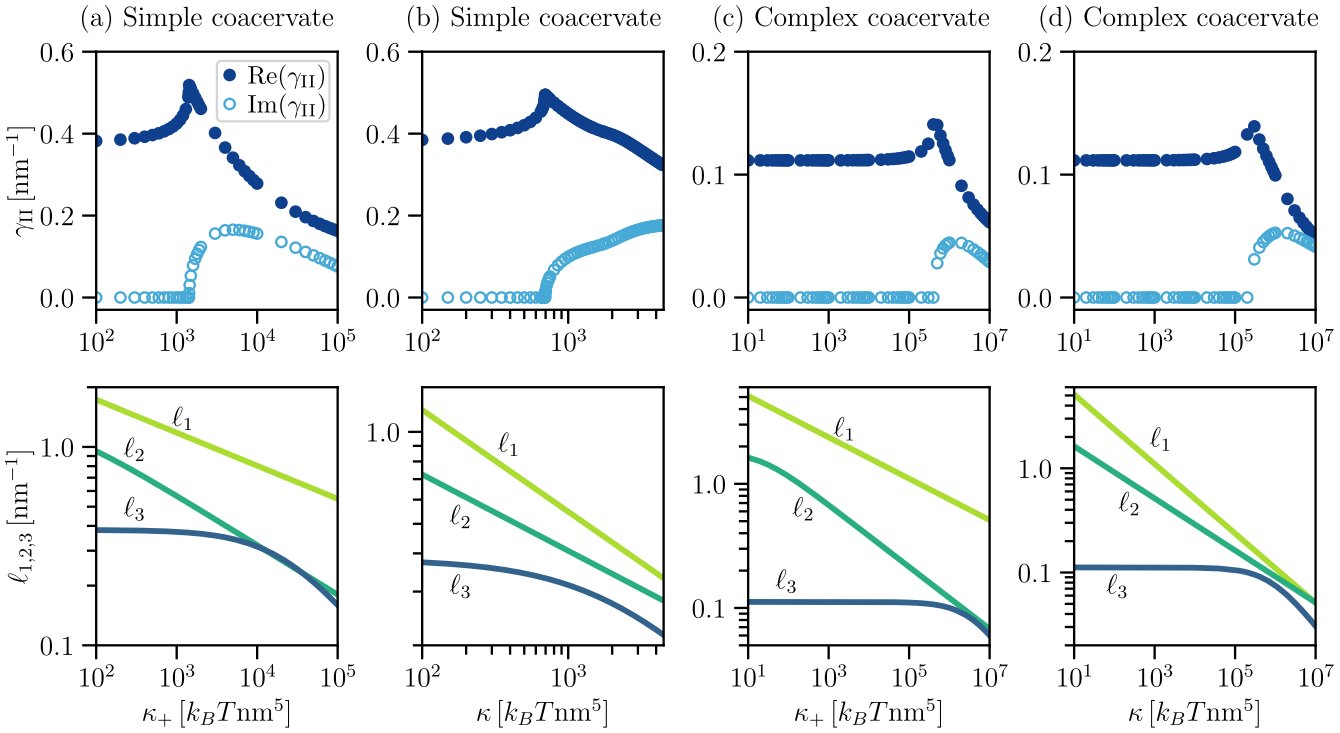

FIG. 8. Change in length scales corresponding to charge oscillations in the dilute phase. Upper panels: The real and imaginary parts of the characteristic length scales γ_{II} in the dilute phase as functions of the surface parameter(s) for simple [panels (a) and (b)] and complex coacervates [panels (c) and (d)]. In panels (a) and (c), only the surface parameter κ_+ is varied, keeping $\kappa_- = 10\,k_BT$ nm^5 fixed. In contrast, panels (b) and (d) show the behavior of γ_{II} when both the surface parameters $\kappa_+ = \kappa_- = \kappa$ are varied. In both cases, one sees that the decay constant turns complex from real with increasing surface parameters, or equivalently, with increasing interfacial width. Lower panels: Log-log plots showing the variations of the length scales ℓ_1, ℓ_2, and ℓ_3 defined in Eq. (B14) corresponding to the situations considered in the respective upper panel. As one can identify, in each case the length scale ℓ_3 changes slope around the region where the length scale γ becomes imaginary. The other two length scales, i.e., ℓ_1 and ℓ_2, do not show such changes in their slopes. Unless stated explicitly, all the parameters correspond to those used in Figs. 2 and 6 of the main text for simple and complex coacervates, respectively.

Its solution,

$$\gamma \simeq \pm\frac{1\pm i}{\sqrt{2}}\left(\frac{e^2}{\varepsilon}\left(\frac{q_+^2}{\kappa_+}+\frac{q_-^2}{\kappa_-}\right)\right)^{1/4} \simeq \pm\frac{1\pm i}{\sqrt{2}}\left(4\pi\ell_B k_B T\left(\frac{q_+^2}{\kappa_+}+\frac{q_-^2}{\kappa_-}\right)\right)^{1/4}, \tag{B18}$$

is discussed in the main text in detail; see Eq. (3). Essentially, this solution is complex, implying an oscillatory decay of the quantities in Eqs. (B3)–(B5) as well as of the corresponding charge density, and is due to a competition of the electrostatic interaction and interfacial tension.

Case II: $\kappa^{2+6\alpha} = \kappa^0$. This condition implies $\alpha = -\frac{1}{3}$. However, plugging this value of α in the different terms, one obtains

$$\kappa^{2+6\alpha} = \kappa^0 < \kappa^{1/3} = \kappa^{1+2\alpha},$$

implying that the third term dominates over the other two. Thus, this case cannot take place.

Case III: $\kappa^{1+2\alpha} = \kappa^0$. Solving this, one obtains $\alpha = -\frac{1}{2}$, and plugging this back into Eq. (B9) leads to the simplified form

$$e^2(q_+^2\kappa_- + q_-^2\kappa_+)\gamma^2 + e^2(2bq_+q_- - q_+^2 d - q_-^2 a) \simeq 0.$$

The solution $\gamma \simeq \pm\sqrt{\frac{q_+^2 d+q_-^2 a-2bq_+q_-}{q_+^2\kappa_-+q_-^2\kappa_+}}$ of this quadratic equation can never be complex. It is either real or purely imaginary, and stems from a competition of short-range Flory-Huggins interactions and the interfacial tension.

b. Small gradient costs

For small gradient costs, i.e., for $\kappa_\pm \to 0$, Eq. (B9) simplifies to

$$\varepsilon(ad - b^2)\gamma^2 + e^2(2bq_+q_- - q_+^2 d - q_-^2 a) \simeq 0,$$

and the resulting decay rate $\gamma \simeq \pm\sqrt{\frac{e^2(q_+^2 d+q_-^2 a-2bq_+q_-)}{\varepsilon(ad-b^2)}}$, originating due to a competition of the electrostatics and short-range Flory-Huggins interactions, is either real or purely imaginary. Therefore, one cannot obtain oscillatory profiles in the sharp-interface limit.

APPENDIX C: TOTAL CHARGE Q INSIDE THE COACERVATE PHASE

In Fig. 9 we plot the total charge $Q = \int_{-\infty}^{0} dx\rho(x)$ contained inside the coacervate phase for three different cases (simple coacervates with or without salt and complex coacervates). As one can see, in all three cases, the total

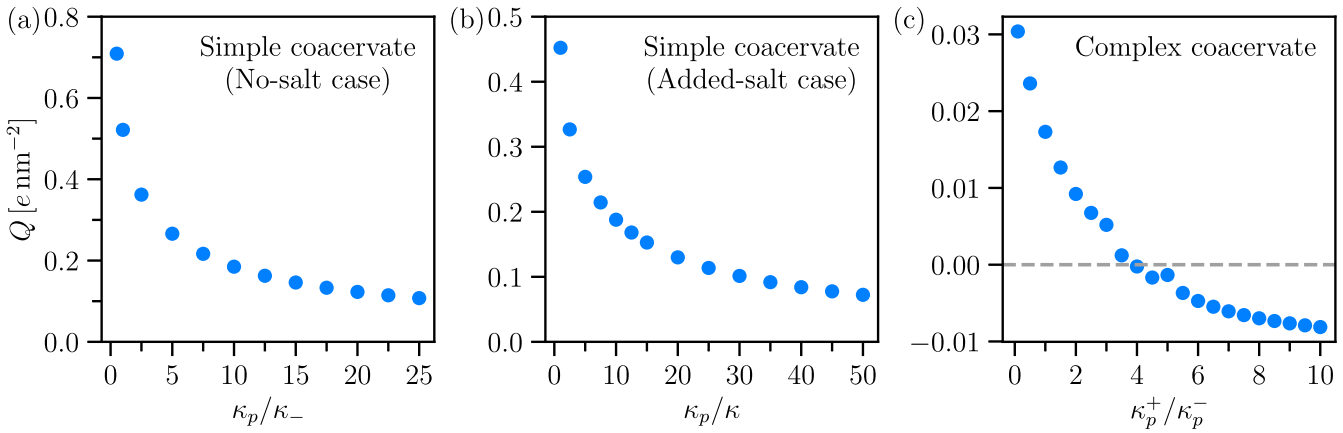

FIG. 9. Variation of both the total charge contained within the coacervate phase as a function of the relative gradient cost parameters for (a) simple coacervates without salt, (b) simple coacervates with salt, as well as for (c) complex coacervates. Whereas for the simple coacervates the total charge of the coacervate remains of the same sign with changing relative gradient cost, for complex coacervates it can even change sign.

charge Q decreases with increasing gradient cost ratios. In addition, it can even flip sign for complex coacervates. The kinks in the curve corresponding to complex coacervates [Fig. 9(c)] correspond to changes in the shape of the electrostatic potential profiles as depicted in Fig. 6(c). We note that the position of the interface, i.e., the location $x = 0$, is defined based on the electrostatic potential profiles. In case the potential profile encounters the value $\psi_D/2$ more than once, we choose the middle one to be the location of the interface.

[1] A. A. Hyman, C. A. Weber, and F. Jülicher, Liquid-liquid phase separation in biology, Annu. Rev. Cell Dev. Biol. **30**, 39 (2014).

[2] Y. Shin and C. P. Brangwynne, Liquid phase condensation in cell physiology and disease, Science **357**, eaaf4382 (2017).

[3] H. L. Booij and H. G. Bungenberg de Jong, *Biocolloids and Their Interactions*, 1st ed. (Springer, Vienna, 1956).

[4] A. I. Oparin, *The Origin of Life on the Earth*, 3rd ed. (Academic Press Inc., New York, 1957).

[5] J. W. Szostak, D. P. Bartel, and P. L. Luisi, Synthesizing life, Nature (London) **409**, 387 (2001).

[6] G. Bartolucci, A. C. Serrão, P. Schwintek, A. Kühnlein, Y. Rana, P. Janto, D. Hofer, C. B. Mast, D. Braun, and C. A. Weber, Sequence self-selection by cyclic phase separation, Proc. Natl. Acad. Sci. USA **120**, e2218876120 (2023).

[7] C. P. Brangwynne, C. R. Eckmann, D. S. Courson, A. Rybarska, C. Hoege, J. Gharakhani, F. Jülicher, and A. A. Hyman, Germline p granules are liquid droplets that localize by controlled dissolution/condensation, Science **324**, 1729 (2009).

[8] J. Guillén-Boixet, A. Kopach, A. S. Holehouse, S. Wittmann, M. Jahnel, R. Schlüßler, K. Kim, I. R. Trussina, J. Wang, D. Mateju, I. Poser, S. Maharana, M. Ruer-Gruß, D. Richter, X. Zhang, Y.-T. Chang, J. Guck, A. Honigmann, J. Mahamid, A. A. Hyman *et al.*, RNA-induced conformational switching and clustering of G3BP drive stress granule assembly by condensation, Cell **181**, 346 (2020).

[9] A. W. Fritsch, A. F. Diaz-Delgadillo, O. Adame-Arana, C. Hoege, M. Mittasch, M. Kreysing, M. Leaver, A. A. Hyman, F. Jülicher, and C. A. Weber, Local thermodynamics govern formation and dissolution of *Caenorhabditis elegans* P granule condensates, Proc. Natl. Acad. Sci. **118**, e2102772118 (2021).

[10] S. F. Banani, H. O. Lee, A. A. Hyman, and M. K. Rosen, Biomolecular condensates: Organizers of cellular biochemistry, Nat. Rev. Mol. Cell Biol. **18**, 285 (2017).

[11] T. M. Franzmann and S. Alberti, Protein phase separation as a stress survival strategy, Cold Spring Harbor Perspect. Biol. **11**, a034058 (2019).

[12] T. M. Franzmann, M. Jahnel, A. Pozniakovsky, J. Mahamid, A. S. Holehouse, E. Nüske, D. Richter, W. Baumeister, S. W. Grill, R. V. Pappu, A. A. Hyman, and S. Alberti, Phase separation of a yeast prion protein promotes cellular fitness, Science **359**, eaao5654 (2018).

[13] T. Lu and E. Spruijt, Multiphase complex coacervate droplets, J. Am. Chem. Soc. **142**, 2905 (2020).

[14] L. M. Jawerth, M. Ijavi, M. Ruer, S. Saha, M. Jahnel, A. A. Hyman, F. Jülicher, and E. Fischer-Friedrich, Salt-dependent rheology and surface tension of protein condensates using optical traps, Phys. Rev. Lett. **121**, 258101 (2018).

[15] L. Hubatsch, L. M. Jawerth, C. Love, J. Bauermann, T. D. Tang, S. Bo, A. A. Hyman, and C. A. Weber, Quantitative theory for the diffusive dynamics of liquid condensates, Elife **10**, e68620 (2021).

[16] P. M. McCall, K. Kim, A. W. Fritsch, J. Iglesias-Artola, L. Jawerth, J. Wang, M. Ruer, J. Peychl, A. Poznyakovskiy, J. Guck, S. Alberti, A. A. Hyman, and J. Brugués, Quantitative phase microscopy enables precise and efficient determination of biomolecular condensate composition, bioRxiv (2023).

[17] M. Abbas, W. P. Lipiński, J. Wang, and E. Spruijt, Peptide-based coacervates as biomimetic protocells, Chem. Soc. Rev. **50**, 3690 (2021).

[18] J. T. G. Overbeek and M. J. Voorn, Phase separation in polyelectrolyte solutions, Theory of complex coacervation, J. Cell. Comp. Physiol. **49**, 7 (1957).

[19] M. Boström, D. R. M. Williams, and B. W. Ninham, Specific ion effects: Why DLVO theory fails for biology and colloid systems, Phys. Rev. Lett. **87**, 168103 (2001).

[20] R. M. Adar, T. Markovich, and D. Andelman, Bjerrum pairs in ionic solutions: A Poisson-Boltzmann approach, J. Chem. Phys. **146**, 194904 (2017).

[21] Edited by D. S. Dean, J. Dobnikar, A. Naji, and R. Podgornik, *Electrostatics of Soft and Disordered Matter*, 1st ed. (CRC Press, Taylor & Francis Group, Boca Raton, FL, 2014).

[22] T. Markovich, D. Andelman, and R. Podgornik, Charged membranes: Poisson–Boltzmann theory, the DLVO paradigm, and beyond, in *Handbook of Lipid Membranes*, edited by C. R. Safynia and J. O. Raedler (Taylor & Francis, London, 2021).

[23] E. Spruijt, J. Sprakel, M. A. Cohen Stuart, and J. van der Gucht, Interfacial tension between a complex coacervate phase and its coexisting aqueous phase, Soft Matter **6**, 172 (2010).

[24] P. R. Banerjee, A. N. Milin, M. M. Moosa, P. L. Onuchic, and A. A. Deniz, Reentrant phase transition drives dynamic substructure formation in ribonucleoprotein droplets, Angew. Chem. Int. Ed. **56**, 11354 (2017).

[25] I. Alshareedah, G. M. Thurston, and P. R. Banerjee, Quantifying viscosity and surface tension of multicomponent protein-nucleic acid condensates, Biophys. J. **120**, 1161 (2021).

[26] T. J. Welsh, G. Krainer, J. R. Espinosa, J. A. Joseph, A. Sridhar, M. Jahnel, W. E. Arter, K. L. Saar, S. Alberti, R. Collepardo-Guevara, and T. P. J. Knowles, Surface electrostatics govern the emulsion stability of biomolecular condensates, Nano Lett. **22**, 612 (2022).

[27] A. Agrawal, J. F. Douglas, M. Tirrell, and A. Karim, Manipulation of coacervate droplets with an electric field, Proc. Natl. Acad. Sci. USA **119**, e2203483119 (2022).

[28] M. van Haren, B. Visser, and E. Spruijt, Probing the surface charge of condensates using microelectrophoresis, Nat. Commun. **15**, 3564 (2024).

[29] M. Vis, V. F. D. Peters, E. M. Blokhuis, H. N. W. Lekkerkerker, B. H. Erné, and R. H. Tromp, Decreased interfacial tension of demixed aqueous polymer solutions due to charge, Phys. Rev. Lett. **115**, 078303 (2015).

[30] P. Zhang and Z.-G. Wang, Interfacial structure and tension of polyelectrolyte complex coacervates, Macromolecules **54**, 10994 (2021).

[31] A. Onuki, Ginzburg-Landau theory of solvation in polar fluids: Ion distribution around an interface, Phys. Rev. E **73**, 021506 (2006).

[32] A. A. Aerov, A. R. Khokhlov, and I. I. Potemkin, Interface between ionic and nonionic liquids: Theoretical study, J. Phys. Chem. B **111**, 3462 (2007).

[33] O. Adame-Arana, C. A. Weber, V. Zaburdaev, J. Prost, and F. Jülicher, Liquid phase separation controlled by pH, Biophys. J. **119**, 1590 (2020).

[34] A. Majee, M. Bier, R. Blossey, and R. Podgornik, Charge symmetry broken complex coacervation, Phys. Rev. Res. **2**, 043417 (2020).

[35] G. L. Celora, R. Blossey, A. Münch, and B. Wagner, Counterion-controlled phase equilibria in a charge-regulated polymer solution, J. Chem. Phys. **159**, 184902 (2023).

[36] J. W. Cahn and J. E. Hilliard, Free energy of a nonuniform system, I. Interfacial free energy, J. Chem. Phys. **28**, 258 (1958).

[37] S. Safran, *Statistical Thermodynamics of Surfaces, Interfaces, and Membranes*, 1st ed. (CRC Press, Taylor & Francis Group, Boca Raton, FL, 2018).

[38] C. A. Weber, D. Zwicker, F. Jülicher, and C. F. Lee, Physics of active emulsions, Rep. Prog. Phys. **82**, 064601 (2019).

[39] D. Deviri and S. A. Safran, Physical theory of biological noise buffering by multicomponent phase separation, Proc. Natl. Acad. Sci. **118**, e2100099118 (2021).

[40] J. R. Casey, S. Grinstein, and J. Orlowski, Sensors and regulators of intracellular pH, Nat. Rev. Mol. Cell Biol. **11**, 50 (2010).

[41] A. Kurotani, A. A. Tokmakov, K.-I. Sato, V. E. Stefanov, Y. Yamada, and T. Sakurai, Localization-specific distributions of protein pi in human proteome are governed by local pH and membrane charge, BMC Mol. Cell Biol. **20**, 36 (2019).

[42] A. J. Bray, Theory of phase-ordering kinetics, Adv. Phys. **51**, 481 (2002).

[43] V. S. Bagotsky, *Fundamentals of Electrochemistry*, 3rd ed. (Wiley, Hoboken, NJ, 2006).

[44] M. Vis, V. F. D. Peters, R. H. Tromp, and B. H. Erné, Donnan potentials in aqueous phase-separated polymer mixtures, Langmuir **30**, 5755 (2014).

[45] J. N. Israelachvili, *Intermolecular and Surface Forces* (Academic Press, Amsterdam, 2011).

[46] L. Leibler, Theory of microphase separation in block copolymers, Macromolecules **13**, 1602 (1980).

[47] A. N. Semenov, Contribution to the theory of microphase layering in block-copolymer melts, Zh. Eksp. Teor. Fiz. **88**, 1242 (1985) [Sov. Phys. JETP **61**, 733 (1985)].

[48] T. Ohta and K. Kawasaki, Equilibrium morphology of block copolymer melts, Macromolecules **19**, 2621 (1986).

[49] V. Y. Borue and I. Y. Erukhimovich, A statistical theory of weakly charged polyelectrolytes: Fluctuations, equation of state and microphase separation, Macromolecules **21**, 3240 (1988).

[50] J. Joanny and L. Leibler, Weakly charged polyelectrolytes in a poor solvent, J. Phys. France **51**, 545 (1990).

[51] L. Leibler, Block copolymers at interfaces, Physica A **172**, 258 (1991).

[52] J. Wittmer and J. Joanny, Charged diblock copolymers at interfaces, Macromolecules **26**, 2691 (1993).

[53] A. M. Rumyantsev, E. Y. Kramarenko, and O. V. Borisov, Microphase separation in complex coacervate due to incompatibility between polyanion and polycation, Macromolecules **51**, 6587 (2018).

[54] A. M. Rumyantsev and J. J. de Pablo, Microphase separation in polyelectrolyte blends: Weak segregation theory and relation to nuclear "pasta," Macromolecules **53**, 1281 (2020).

[55] D. J. Grzetic, K. T. Delaney, and G. H. Fredrickson, Electrostatic manipulation of phase behavior in immiscible charged polymer blends, Macromolecules **54**, 2604 (2021).

[56] G. H. Fredrickson, S. Xie, J. Edmund, M. L. Le, D. Sun, D. J. Grzetic, D. L. Vigil, K. T. Delaney, M. L. Chabinyc, and R. A. Segalman, Ionic compatibilization of polymers, ACS Polym. Au **2**, 299 (2022).

[57] F. J. Solis and M. O. de la Cruz, Surface-induced layer formation in polyelectrolytes, J. Chem. Phys. **110**, 11517 (1999).

[58] M. Bier, A. Gambassi, and S. Dietrich, Local theory for ions in binary liquid mixtures, J. Chem. Phys. **137**, 034504 (2012).

[59] N. Gavish and A. Yochelis, Theory of phase separation and polarization for pure ionic liquids, J. Phys. Chem. Lett. **7**, 1121 (2016).

[60] R. Kjellander and D. Mitchell, An exact but linear and Poisson-Boltzmann-like theory for electrolytes and colloid dispersions in the primitive model, Chem. Phys. Lett. **200**, 76 (1992).

[61] P. Attard, Asymptotic analysis of primitive model electrolytes and the electrical double layer, Phys. Rev. E **48**, 3604 (1993).

[62] A. A. Aerov, A. R. Khokhlov, and I. I. Potemkin, Microphase separation in a mixture of ionic and nonionic liquids, J. Phys. Chem. B **111**, 10189 (2007).

[63] R. L. de Carvalho and R. Evans, The decay of correlations in ionic fluids, Mol. Phys. **83**, 619 (1994).

[64] A. M. Smith, A. A. Lee, and S. Perkin, The electrostatic screening length in concentrated electrolytes increases with concentration, J. Phys. Chem. Lett. **7**, 2157 (2016).

[65] H. Nikaido, Porins and specific channels of bacterial outer membranes, Mol. Microbiol. **6**, 435 (1992).

[66] G. M. Geise, H. J. Cassady, D. R. Paul, B. E. Logan, and M. A. Hickner, Specific ion effects on membrane potential and the permselectivity of ion exchange membranes, Phys. Chem. Chem. Phys. **16**, 21673 (2014).

[67] K. K. Nakashima, M. H. van Haren, A. A. André, I. Robu, and E. Spruijt, Active coacervate droplets are protocells that grow and resist Ostwald ripening, Nat. Commun. **12**, 3819 (2021).

[68] S. Chen and Z.-G. Wang, Charge asymmetry suppresses coarsening dynamics in polyelectrolyte complex coacervation, Phys. Rev. Lett. **131**, 218201 (2023).

[69] M. Tena-Solsona, J. Janssen, C. Wanzke, F. Schnitter, H. Park, B. Rieß, J. M. Gibbs, C. A. Weber, and J. Boekhoven, Accelerated ripening in chemically fueled emulsions, ChemSystemsChem **3**, e2000034 (2021).

[70] T.-Y. D. Tang, M. Antognozzi, J. A. Vicary, A. W. Perriman, and S. Mann, Small-molecule uptake in membrane-free peptide/nucleotide protocells, Soft Matter **9**, 7647 (2013).

[71] B. Ghosh, R. Bose, and T. D. Tang, Can coacervation unify disparate hypotheses in the origin of cellular life? Curr. Opin. Colloid Interface Sci. **52**, 101415 (2021).

[72] R. Kubota, S. Torigoe, and I. Hamachi, Temporal stimulus patterns drive differentiation of a synthetic dipeptide-based coacervate, J. Am. Chem. Soc. **144**, 15155 (2022).

[73] J. Bauermann, G. Bartolucci, J. Boekhoven, C. A. Weber, and F. Jülicher, Formation of liquid shells in active droplet systems, Phys. Rev. Res. **5**, 043246 (2023).

[74] A. M. Bergmann, J. Bauermann, G. Bartolucci, C. Donau, M. Stasi, A.-L. Holtmannspoetter, F. Julicher, C. A. Weber, and J. Boekhoven, Liquid spherical shells are a non-equilibrium steady state of active droplets, Nat. Commun. **14**, 6552 (2023).

[75] I. M. Lifshitz, Some problems of the statistical theory of biopolymers, Zh. Eksp. Teor. Fiz. **55**, 2408 (1969) [Sov. Phys. JETP **28**, 1280 (1969)].

[76] I. M. Lifshitz, A. Y. Grosberg, and A. R. Khokhlov, Some problems of the statistical physics of polymer chains with volume interaction, Rev. Mod. Phys. **50**, 683 (1978).

[77] P. G. de Gennes, Dynamics of fluctuations and spinodal decomposition in polymer blends, J. Chem. Phys. **72**, 4756 (1980).

[78] A. Johner and J. Joanny, Polymer adsorption in a poor solvent, J. Phys. II France **1**, 181 (1991).